

STRUCTURAL AND LUMINOUS PROPERTIES OF SYNTHESIZED PEROVSKITE – TYPE OXIDE USING ALGINATE

K. KARTHIKEYAN^a, A. THIRUMOORTHY^{b*}

^a*Research and Development centre, Bharathiar University, Coimbatore, Tamilnadu, India.*

Present address: Guest Lecturer, Department of chemistry, Government Arts College, Udumalpet – 642 126, Tamilnadu, India.

^b*Assistant Professor, Post Graduate Department of Chemistry, Government Arts College, Udumalpet – 642 126, Tamilnadu, India.*

Synthesis of perovskite - type oxides like Bismuth Ferrite (BFO) was carried out using alginate as a supporter followed by annealing at 500°C to obtain pure phase of BFO. The structural morphology, bonding character, and specific capacitance have been studied by UV- Visible, FT - IR, X-ray diffraction, Scanning electron microscopy and Cyclic Voltammetric studies. The alginate used support for the formation of pure BiFeO₃ nanoparticles at 500°C for 1 h without any secondary phases observed in XRD. The band gap is calculated using Tauc's plot and was found to be 1.67 eV. The Photoluminescence studies shows that the doublet peaks formed in the range of 400 - 450 nm besides peak shifted to lower range since absence of secondary phases. FT - IR spectra shows the presence of M-O bond in the range of 400-600 cm⁻¹ and above 600 cm⁻¹ elaborates O-H bending and trapped NO₃²⁻ bonds. The SEM images shows that agglomerated BiFeO₃ nanoparticles are formed and the electrochemical studies revealed that good cyclic property at 1M NaOH aqueous solution and found to be the comparable specific capacitance of 140 Fg⁻¹.

(Received August 10, 2016; Accepted Accepted October 29, 2016)

Keywords: BFO nanoparticles; Sol- gel process; Alginate; capacitors.

1. Introduction

Bismuth Ferrites are deft single multi-ferroic materials with high Curie temperature of 1103 K and Neel temperature of 643K [1]. Generally, BFO have been used for various fields such as data storage, spintronics [2], photovoltaic devices [3,4]and gave main attention in the degradation of azo dyes, triphenyl methane dyes, Rhodamine-B [5 – 7], in addition to photo catalytic activity for the degradation of organic compounds [8 – 10]. Although BFO possess such immense properties, they have some adverse residing difficult, created due to the secondary phase formation of BFO. Veterans used various ways for improving the properties of doped materials, with different types of promoters and synthetic routes. Tayyebe et al., [11] reported that ultrasonication method for producing pure material of BFO. Yumin Han et al., [12] observed that enhanced percentage of Co and Er indicates the presence of minor amount of impurities such as Bi₄O₇. Also, David Diaz used tartaric acid and glycine as promoters at various annealing temperatures to prepare high pure BFO [13]. Hence, several reports indicate that the synthesis of pure BFO is a great task, since it produces some amount of impurities. Researchers have been used tartaric acid, citric acid, glycine as supporters to prepare pure BFO and acetic acid have also been used to remove the secondary phases.

In this research article, our aim is to use alginic acid for synthetic approach as carboxyl and hydroxyl groups are present in this polymer, form a complex with metal ions and provide a good environment for controlled growth of nanoparticles within the polymeric network. Based on this, biopolymers such as agar, cellulose, DNA [14,15], chitosan [16], starch [17], dextran [18],

* Corresponding author: dramoorthiudt@gmail.com

and gelatine [19,20] have been used for synthesis of various metal nanoparticles and semiconductors. So, we need an efficient way to remove secondary phase of BFO exploit biopolymers. On the basis of low toxicity and biocompatibility of alginate, it is used widely in various application fields such as drug release [21], water purification [22], catalysis [23], wound dressings [24, 25], drug carriers and tissue scaffolds [26, 27] and hence we attempted. Alginate is a binary linear hetero polymer consists of 1,4 – linked β -D-mannuronic acid and α -L-guluronic acid units [28] as shown in Figure 1, has immense ability to allow specifically metal ion into a polymeric structure in which carboxylate group involve as part of attracting metal ions.

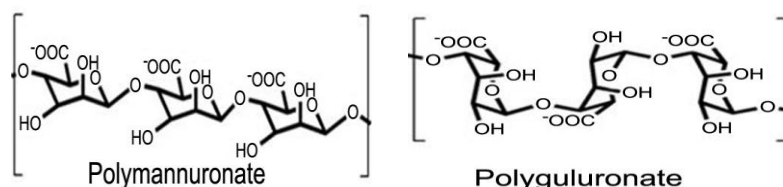


Fig. 1. Structure of alginate matrix.

Alginate is a low viscosity hydro-gel, has mild reducing ability and low prices shown to be good stabilizer for synthesis of metal nanoparticles [29]. The main objective of this work is to synthesis single phase BFO and most commonly secondary species have to be removed using alginate as promoter material. The formation of polycrystalline phases during synthesis and developed pure BiFeO₃ nano crystals at 500°C. The characterization of BFO was carried out by UV- Visible, FT- IR, XRD, SEM, PL, and cyclic voltammetry for interpretation, have been discussed.

2. Experimental Section

2.1 Materials and methods

Bismuth nitrate, Iron nitrate, Sodium alginate (from Merck, Germany) are all analytical grades and were used without further purification. Deionized water was used in the sample preparation.

2.2. Preparation of BFO

BFO nanoparticles were prepared by using equimolar solution of bismuth nitrate [Bi(NO₃)₃·5H₂O] and iron nitrate [Fe(NO₃)₃·9H₂O] in 40 ml of deionized water and 2% of alginate was added followed by 1.2 ml of nitric acid with constant stirring at room temperature for half an hour. The mixture was heated until all the solvents evaporated and combustion reaction took place. The brown powder was obtained and it is annealed in a muffle furnace at 500°C in air for 1 h. The dried sample was used for further characterization.

2.3. Characterization

IR spectra were recorded with FT-IR spectrophotometer (IR Prestige-21, Shimadzu) and Double beam UV-Vis spectrophotometer (UV-1800, Shimadzu) equipped UV-Probe software, has been employed for recording the UV-Vis spectra. Fluorescence spectra were recorded on a Horiba Jobin Yvon spectrofluorophotometer (Fluorolog-3). X-ray diffraction patterns were recorded on a Shimadzu labX-6000 diffractometer with Cu K α radiation ($\lambda = 1.54\text{\AA}$). SEM images were taken on a SEM JEOL model JSM 6390 with an accelerating voltage of 20 kV. The cyclic voltammetric experiments were carried out with a computer-controlled electrochemical system (CH1660C Electrochemical Analyzer) between the scan rate of 10 mV s⁻¹ and 50 mV s⁻¹.

3. Results and discussion

3.1 UV- Visible Spectra

UV- Vis spectra of BFO nanoparticles prepared at 500°C is shown in Figure 2 (b). Band gap was calculated from the point of inflection in the first derivative plot of the UV–Vis absorption spectra of Nanoparticles system. The band gap estimated by extrapolating Tauc 's plot and the linear portion of $(\alpha h\nu)^2$ against $h\nu$ plot to the point $\alpha = 0$ and was found to be 1.67 eV. The aqueous solution of sodium alginate possess the absorption band around 260 nm [30], which is due to double bonds of alginate formed after the main chain fission of the polymer shown in Figure 2 (a).

In our study the UV-Vis spectra obtained at about 365 nm confirmed that sodium alginate and metal ions Bi and Fe involving in the interaction gives shoulder peak in visible region [31]. This indicates that alginate molecules support strongly for wholesome formation of BFO nanoparticles. UV-Vis spectra also reveals that the BFO gave a broad red shift peak at about 450-750 nm which clearly proved that the particle size has been enlarged shown by XRD and SEM. Also, the optical studies supported that alginate involves strongly in the formation of BFO NPs.

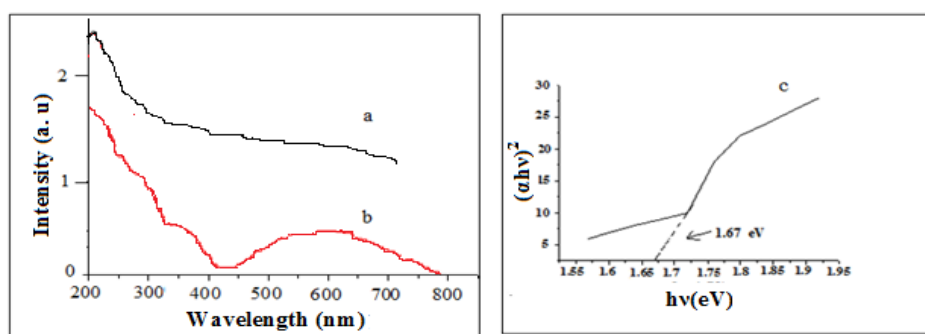


Fig. 2. UV – Visible spectrum of (a) Sodium alginate (b) Na-Alg BFO nano particles (c) Band gap calculation of BFO Nps.

3.2 XRD analysis

X- ray diffraction pattern of BFO nanoparticles gives main peak at $2\theta = 32.05^\circ$ for the planes 104 and 110 confirmed that the crystalline size was 123 nm by Scherrer equation shown in Figure 3. Usually, the by-products like β - Bi_2O_3 formed during the synthesis of BFO Nps were removed by washing with strong acids like nitric acid which could dissolve BiFeO_3 . Recently, David Diaz et al. [13] found that weak acids such as acetic acid can also be used for purification and the impurities of bismuth oxide gave peaks at $2\theta = 27.9^\circ$ and 28.20° for β - Bi_2O_3 and $\text{Bi}_2\text{Fe}_4\text{O}_9$ respectively.

In our present work, the synthesized alginate supported BFO was not washed with any strong as well as weak acids, but it gives neither peak at $2\theta = 27.9^\circ$ nor 28.20° indicating the absence of secondary phases. Consequently, the XRD pattern proves that BFO NPs are highly pure crystalline and possess intense peak at $2\theta = 32.05^\circ$.

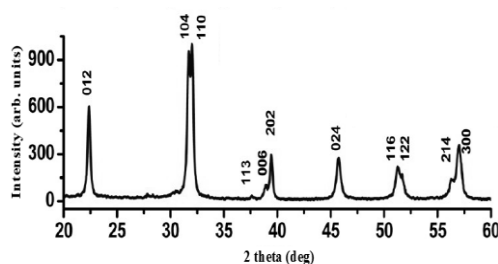


Fig. 3. XRD pattern of BFO nanoparticles

3.3 Scanning Electron Microscopy

The SEM images of agglomerated BFO nanoparticles are shown in Figure 4. This agglomeration of BFO NPs is due to narrow distance between surface of nanoparticles caused by attractive Vander Waals forces and the driving force that tends to minimize the total surface energy of the system [32]. Chih-Yu Wang [33] suggested that gold alginate composites form a smoother surface spheres with diameter of 10 – 20 nm and Parani Sundarrajan [31] reported that spherical shape of alginate stabilized zinc, cadmium and lead nano composites with the average crystallite size of 1.8 to 4.8 nm are formed. Kamyar Shameli et al., [34] found that the exterior surface of [Ag(Alg)] become shiny in the spots spherical shapes with diameter less than 20 nm. This confirmed the uniform shape and size of BFO nanoparticles have been formed and the size of the particle is about 105nm.

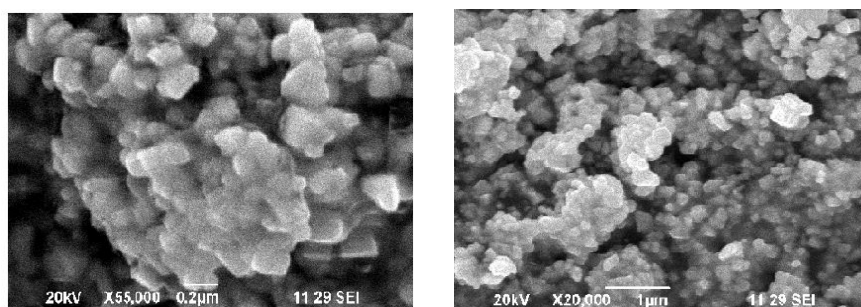


Fig. 4. SEM images of BFO nanoparticles

3.4 Photoluminescence studies

PL spectra of Perovskite type bismuth iron oxide using alginate was measured in the range from 350 to 650 nm is shown in Figure 5. This gives two intense peaks in the range of 400 – 450 nm. Yao et al., [35] reported that the bulk BFO exhibited an emission band centered at 400 nm and a shoulder peak appeared at 550 nm. Also, they found that KNSBN/BFO/KNSBN (SBS) and BFO/KNSBN/BFO (BSB) tri layer films with different phases, multiple band gap energies were obtained. This multiple band gap energies can be approximated as the combination of the band gap energy of potassium sodium strontium barium niobate (KNSBN) and BFO films. Mishra et al., [36] suggested that defects or impurity levels arise in longer wave length. According to principle, pure BFO only has the intrinsic emission arising from the band-to-band transitions. Any other emission of longer wavelengths must come from various defects and / or impurity levels inside the band gap. In Figure 5, the two peaks were obtained at 415 and 440 nm with band gap of 2.98 eV and 2.81 eV respectively. This suggests that in BFO NPs the peak at 415 nm corresponds to regular emission band for electron transition between valence and conduction band. Further an intense emission band for oxygen vacancies [37], is shifted to lower wave length of 440nm indicating that no impurities were present in synthesised BFO NPs.

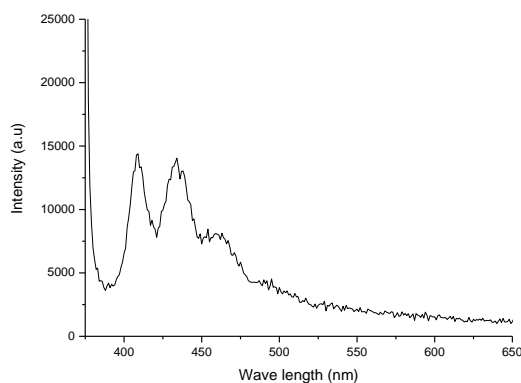


Fig. 5. Photoluminescence of BFO nanoparticles

3.5 FT-IR Spectra

BFO NPs were prepared and annealed at 500°C for 1h and the FT - IR spectra was recorded using KBr pellets and is shown in Figure 6. This spectrum does not exhibit any peak at about 3500 cm⁻¹ indicating that the nanoparticles were dehydrated. However, it gives an intense peak at 1514 cm⁻¹ due to bending vibration of H₂O and a strong peak at 840 cm⁻¹ clearly indicates that traces of trapped NO₃⁻ ions in the BFO nanoparticles [38]. The peak obtained at 1381 cm⁻¹ was attributed due to trapped nitrates [39]. Moreover, IR absorption peaks at about 567 cm⁻¹ and 420 cm⁻¹ were due to Fe-O stretching and bending vibrations respectively [40].

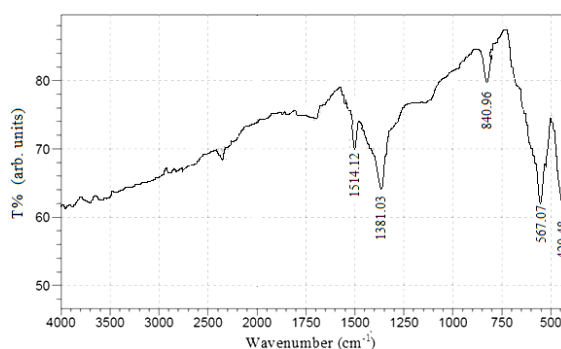


Fig. 6. FT-IR spectrum of BFO nanoparticles

3.6 CV Studies

The crucial characteristics of a supercapacitor device are specific energy storage and specific power that can be delivered to the load along with its cycling life, self discharge current and efficiency. The specific capacitance, Sc , is determined by the equation,

$$Sc = C / W$$

Where W is the weight of the active material on the substrate and C is the average capacitance [41].

Carbon in various modifications is the electrode material used most frequently for electrodes of electrochemical capacitors [42]. The reasons for using carbon are low cost, high surface area, availability, and established electrode production technologies. Carbons are available with a specific surface area of up to 3000 m² g⁻¹ as powders, woven cloths, felts, nanotubes, aerogel or fibres. Charge storage on carbon electrodes is predominantly capacitive in the electrochemical double layer. There are however, contributions from surface functional groups which are in general present on activated carbons and which can be charged and discharged giving rise to capacitance. The effect of surface functional groups containing oxygen on the stability of carbon electrodes in super capacitors using organic electrolyte was investigated by Nakamura et al., [43]. In general, one can observe that both the stability and conductivity of the activated high surface area carbon decreases with increasing surface area. Most of the today's commercial devices use activated carbon based electrodes in organic electrolytes with cell operating voltages up to 2.7 V with capacitance about 100 Fg⁻¹. Specific capacitance values obtained with CNT and aerogel ranged from 20 to 100 Fg⁻¹ [44]. Due to cost consideration, cheaper transition metal oxide candidates with good capacitive values have attracted much attention.

Lokhande et al., [45] reported that BiFeO₃ has better performance in NaOH electrolyte in comparison with other electrolytes and the increased concentration of NaOH (0.5 — 1.0M) gives well resolved peaks in cyclic voltammograms. This is due to free electrolyte starvation since, for the amount of electrolyte present in that solution and hence almost all of its ions become adsorbed at the high area interface, enhancing the internal resistance effect towards full state of charge and may due to the combination of usual distributed resistance effect [46]. Thus, it was observed that at lower scan rates, inner and outer sites were more active, and full utilization of BFO electrode in NaOH electrolyte solution occurred. Hence, this might help to increase the supercapacitance of

BFO electrode at lower scan rate. At higher scan rates, only outer sites could be more active than inner sites which were unable to participate in the redox reaction in the electrolyte solution [47].

The BiFeO₃ nanocrystalline electrode was an efficient potential candidate for supercapacitor applications [48]. The Specific capacitance of 140 Fg⁻¹ for alginate supported BFO was compared with supercapacitance for Ruthenate pyrochlore pellets obtained by Park et al., [49] (160 F g⁻¹) and Bang et al., [50] (90 - 100 F g⁻¹). These facts confirmed the stable nature of BiFeO₃ electrode.

In our present work, the cyclic voltammetric measurements were employed to explore the BFO electrodes for electrochemical supercapacitor applications with 1M NaOH electrolyte concentration in a conventional three-electrode system. A typical cyclic voltammograms at different scan rate of 10 – 50 mVs⁻¹ between the potentials of + 0.3 and – 0.8 V in aqueous solution of 1M NaOH were performed, is as shown in Figure 7. It has been found that the high specific capacitance is due to the nanostructure in the form of agglomerated particles forms porous morphology and high surface area, which are the prime requirements in supercapacitance applications. The system is quite stable with respect to repeated cycling. BFO system undergoes a redox process with oxygen vacancies being generated giving rise to high specific capacitance. The high specific capacitance coupled with stability at long cycles brings forth its application as electrodes in batteries.

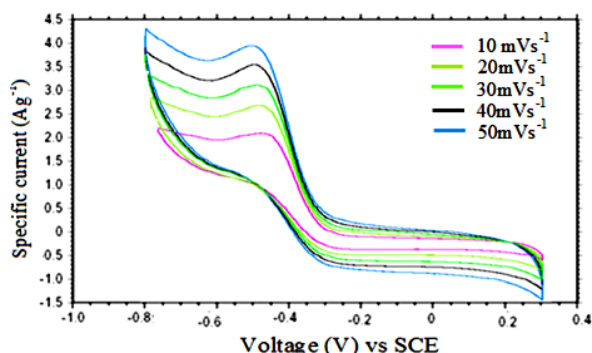


Fig.7. Cyclic Voltammograms of BiFeO₃ in NaOH at different scan rate.

4. Conclusions

BiFeO₃ nanoparticles were successfully synthesized through sol-gel method using alginate as a supporter followed by annealing at 500°C. From UV-visible spectra, it has been confirmed that the presence of metal- alginate bond formation and the optical band gap was found to be 1.67eV. The presence of metal - oxygen bond was also confirmed by FT-IR spectra. The average crystalline size was found to be 123 nm through XRD indicates that the non-existence of any secondary phases in the synthesized BFO NPs.

Further, the SEM image of Perovskite type BFO shows agglomeration occurs and the BFO nanoparticles becomes porous in nature. In Photoluminescence, a luminescence peak with shoulder was observed and confirmed the increased purity of BFO. The specific capacitance of BFO was found to be 140 F g⁻¹ and this comparable value of capacitance attributed to the nano structured and high stability of BFO Nps.

References

- [1] V. V. Khikhlovskiy, M.Sc. Thesis Zernike Institute for Advanced Materials, University of Groningen, Groningen, Germany (2010).
- [2] G. Catalan, J. F. Scott, Adv. Mater. **21**, 2463, (2009).
- [3] Y. Zang, D. Xie, X. Wu, Y. Chen, Y. Lin, M. Li, H. Tian, X. Li, Z. Li, H. Zhu, T. Ren, D. Plant, Appl. Phys. Lett. **99**,132904, (2011).

- [4] S. Y. Yang, J. Seidel, S. J. Byrnes, P. Shafer, C. H. Yang, M. D. Rossell, P. Yu, Y. H. Chu, J. F. Scott, J. W. Ager, L. W. Martin, R. Ramesh, *Nat. Nanotechnol.* **5**, 143 (2010).
- [5] M. A. Brown, S. C. De-Vito, *Environ. Sci. Technol.* **23**, 249 (1993).
- [6] I. K. Konstantionou, T. A. Albanis, *Appl. Catal. B- Environ.* **49**, 1 (2004).
- [7] D. Zhao, C. C. Chen, Y. Wang, W. H. Ma, J. C. Zhao, T. Rajh, L. Zang, *Environ. Sci. Technol.* **42**, 308 (2008).
- [8] J. H. Carey, J. Lawrence, H. M. Tosine, *B. Environ. Contam. Tox.* **16**, 697, (1976).
- [9] S. Mozia, P. Brozek, J. Przepiorski, B. Tryba, A.W. Morawki, *J. Nanomater.* **2012**, 10, (2012).
- [10] Y. Han, H. S. Kim, H. Kim, *J. Nanomater.* **2012**, Article ID 427453 10 pages, (2012).
- [11] Tayyabe Solani, Mohammad H. Entezari, *Chem. Eng. J.* **223**, 145 (2013).
- [12] Yumin Han, Weiwei Mao, Chuye Quan, Xingfu Wang, Jianping Yang, Tao Yang, Xing'ao Li, Wei Huang, *Mat. Sci. Eng. B* **188**, 26 (2014).
- [13] José Luis Ortiz- Quiñonez, David Díaz, Inti Zumeta-Dubé, Humberto Arriola-Santamaría, Israel Betancourt, Patricia Santiago-Jacinto, Noel Nava-Etzana, *Inorg. Chem.* **52**, 10306 (2013).
- [14] S. Kundu, H. Lee, H. Liang, *Inorg. Chem.* **48**, 121 (2009).
- [15] N. Ma, J. Yang, K. M. Stewart, S.O. Kelley, *Langmuir* **23**, 12783 (2007).
- [16] Z. Li, Y. Du, Z. Zhang, D. Pang, *React. Funct. Polym.* **55**, 35 (2003).
- [17] O. S. Oluwafemi, O. O. Adeyemi, *Mater. Lett.* **64**, 2310, (2010).
- [18] Y. Y. Kim, D. Walsh, *Nanoscale* **2**, 240 (2010).
- [19] S. J. Byrne, Y. Williams, A. Davies, S. A. Corr, A. Rakovich, Y. K. Gun'ko, Y. P. Rakovich, J. F. Donegan, Y. Volkov, *Small* **3**, 1152, (2007).
- [20] M. Mozafari, Moztarzadeh, *J. Colloid Interf. Sci.* **351**, 442, (2010).
- [21] G. Rangaraj, N. Kishore, U. M. Dhanalekshmi, M. D. Raja, C. Senthil kumar, P. N. Reddy, *J. Pharm. Sci. & Res.* **2**, 77 (2010).
- [22] S. Lin, R. Huang, Y. Cheng, J. Liu, B. L. T Lau, M. R. Wiesner, *Water Res.* **47**, 3959 (2013).
- [23] J. Yang, J. Pan, *Acta Mater.* **60**, 4753, (2012).
- [24] I. Yuvarani, S. S. Kumar, J. Venkatesan, S. K. Kim, P. N. Sudha, *J. Biomater. Tissue Eng.* **2**, 54 (2012).
- [25] P. Marie Arockianathan, S. Sekar, S. Sankar, B. Kumaran, T. P. Sastry, *Carbohydr. Polym.* **90**, 717 (2012).
- [26] C. H Goh, P. W. S Heng, L. W. Chan, *Carbohydr. Polym.* **88**, 1 (2012).
- [27] M. George, T. E. J. Abraham, *Control. Release* **114**, 1 (2006).
- [28] S. K Chanda, E. L Hirst, E. G. Percival, A. G. Ross, *J. Chem. Soc.* 1833, (1952).
- [29] S. V. Otari, R. M. Patil, S. R. Waghmare, S. J. Ghosh, S. H. Pawar, *Dalton Trans.* **42**, 9966 (2013).
- [30] N. Nagasawa, H. Mitomo, F. Yoshii, T. Kume, *Polym. Degrad. Stab.* **69**, 279 (2000).
- [31] Parani Sundarajan, Prabakaran Eswaran, Alexander Marimuthu, Lakshmi Baddireddi Subhadra, Pandian Kannaiyan, *Bull. Korean Chem. Soc.* **33**, 3218 (2012).
- [32] K. Shameli, M. B. Ahmad, P. Shabanzadeh, E. A. J. Al-Mulla, A. Zamanian, Y. Abdollahi, S. D. Jazayeri, M. Eili, F. Aziz Jalilian, *Res. Chem. Intermediat.* **40**, 1313 (2014).
- [33] Chih-Yu wang, Keng-Shiang Huang, chih- Hui Yang, Wan-Ru Chang and Alexandru Mihai Grumezescu, *Int.J. Latest Res. Sci. and Tech.* **3**, 139 (2014).
- [34] Sepideh Keshan Balavandy, Kamyar Shameli, Zurina Zainal Abidin, *Int. J. Electrochem. Sci.* **10**, 486 (2015).
- [35] Y. B Yao, C. L. Mak, *J. Alloy. Compd.* **586**, 448 (2014).
- [36] Dillip K. Mishra, Xiaoding Qi, *J. Alloy. Compd.* **504**, 27 (2010).
- [37] Bobby Singh Soram, Boinis Singh Ngangom, H. B. Sharma, *Thin Solid films* **524**, 57 (2012).
- [38] Glenda Biasotto, Alexandre Z. Simões, César R. Foschini, Selma G. Antônio, Maria A. Zaghete, Jose A. Varela, *Processing and Application of Ceramics* **5**, 3, (2011).
- [39] A. V. Zaleskii, A. A. Frolov, T. A. Khimich, A. A. Bush, *Phys. Solid State*, **45**, 134 (2003).

- [40] Pawan Kumar, Manoranjan Kar, J. Alloy. Compd. **584**, 566 (2014).
- [41] C. D. Lokhande, D. P. Dubal, M. Oh-Shim Joo, Curr. Appl. Phys. **11**, 255 (2011).
- [42] A. G. Pandolfo, A. F. Hollenkamp, J. Power Sources **157**, 11 (2006).
- [43] M. Nakamura, M. Nakanishi, K. J. Yamamoto, Power Sources **60**, 225 (1996).
- [44] P. Simon, A. Burke, Electrochem. Soc. Interface page 38, (Spring 2008).
- [45] C. D. Lokhande, T. P. Gujar, V. R. Shinde, R. S. Mane, S. Han, Electrochem. Commun. **9**, 1805 (2007).
- [46] C. C. Hu, T. W. Tsou, Electrochem. Comm. **4**, 105 (2002).
- [47] Vijaykumar V. Jadhav, Manohar K. Zate, Shude Liu, Mu. Naushad, Rajaram S. Mane, K. N. Hui, Sung-Hwan Han, App. Nanosci. **6**, 4 (2016).
- [48] M. Winter, R. Brodd, Chem. Rev. **104**, 4245 (2005).
- [49] B. O. Park, C. D. Lokhande, H. S. Park, K. D. Jung, O. S. Joo, Mater. Chem. Phys. **86**, 239 (2004).
- [50] H. J. Bang, W. Lu, F. Cao, J. Prakash, Electrochem. Commun. **2**, 653 (2000).